International Journal of Engineering Innovation & Research
Volume 10, Issue 3, ISSN: 2277 – 5668

Analysis of Leakage Permeance of Brushless Electromagnetic and Radial Permanent Magnet Composite Excitation Power Generation Device for Automobile

Mingjun Xu [1], Hongbin Yin [1*], Shilong Yan [1], Yanhong Gao [2], Zhendong Liu [3] and Wenchao Zhang [1]

[1] School of Transportation and Vehicle Engineering, Shandong University of Technology, Zibo City, Shandong Province, 255000, China.

[2] Shandong Tangjun Ouling Automobile Manufacturing Co. Ltd, Zibo City, Shandong Province, 255000, China. [3] School of Physics and Electronic Information, Dezhou University, Dezhou City, Shandong Province, 253000, China.

*Corresponding author email id: hbinyin@163.com

Date of publication (dd/mm/yyyy): 05/07/2021

Abstract **– The equivalent magnetic circuit diagram of brushless claw pole electro excitation rotor and radial permanent magnet rotor is drawn by using the equivalent magnetic circuit method, and the influencing factors of the composite leakage permeance between claw pole of electro excitation rotor, the composite leakage permeance between both end faces of permanent magnet steel of permanent magnet rotor and the leakage permeance between pole shoe and adjacent invisible pole are analyzed, and the measures to suppress the magnetic leakage are taken to reduce the magnetic leakage. Particle swarm optimization algorithm is used to optimize the main structural parameters of the power generation device to obtain the optimal matching parameters. A brushless electromagnetic and radial permanent magnet compound excitation power generation device with low failure rate, high efficiency, high power density, high reliability and stable output voltage is developed.**

Keywords **– Automobile, Leakage Permeance, Brushless Electromagnetic, Radial Permanent Magne-T, Composite Excitation Power Generation Device.**

I. INTRODUCTION

At present, there are mainly silicon rectifier generator and permanent magnet generator used in automobile. Silicon rectifier generator generates magnetic field by electric excitation winding. Most of the electric energy through electric excitation winding is consumed due to the heating of excitation winding, and only part of the electric energy is converted into magnetic energy for power generation, so the utilization rate of electric energy is low; Permanent magnet generator has no excitation loss, high efficiency, high power density and other advantages, but because the permanent magnetic field is not adjustable, its output voltage is proportional to the speed, resulting in low output voltage at low speed and high output voltage at high speed, which affects the normal work of automotive electrical equipment [1, 2].

The brushless electric excitation rotor of the compound excitation stabilized voltage power generation device provides the regulating magnetic field, the current of the excitation winding is small, the excitation loss is small, the permanent magnet rotor provides the main magnetic field, and the NdFeB permanent magnet with high magnetic energy is used for excitation, which increases the power density, therefore, the compound excitation stabilized voltage power generation device with brushless electromagnetic and radial permanent magnet excitation not only has the good regulation characteristics of the electric excitation generator, but also has the advantages of the permanent magnet generator with high power density, high efficiency and high reliability, which is very suitable for the automobile generator.

II. Analysis of Leakage Permeance of the Composite Excitation Power Generation Device

The rotor of the compound excitation generator is composed of brushless claw pole electric excitation rotor and radial permanent magnet rotor. The brushless claw pole electric excitation rotor is composed of front and rear claw poles and excitation winding. The excitation winding is fixed on the stator core through the excitation winding bracket, and does not rotate with the rotating shaft, which realizes brushless and improves the working reliability of the generator. The radial permanent magnet rotor core is composed of long T-shaped salient pole teeth and short T-shaped salient pole teeth arranged at intervals. The permanent magnet steel is installed on the short T-shaped salient pole teeth with non-magnetic screws through pole shoes. In order to prevent the occurrence of magnetic accumulation on the stator teeth and increase the starting resistance moment, each pole is composed of two permanent magnet steels, and there is a gap between the two permanent magnets, the long T-shaped salient pole teeth form the invisible pole structure through the magnetic conductivity of the rotor core, and the material utilization rate is high. The structure diagram of the compound excitation voltage stabilizing power generation device is shown in Fig. 1.

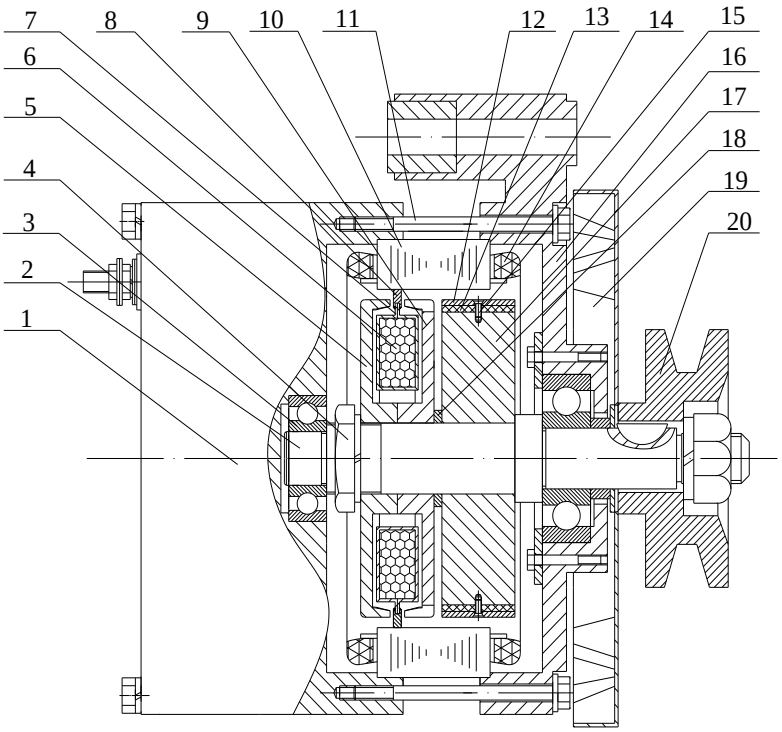

Fig. 1. Structural schematic diagram of the compound excitation stabilized voltage power generation device.

1. Rear end cover; 2. Rotating shaft; 3. Bearing; 4. Lock nut; 5. Posterior claw pole; 6. Electric excitation winding; 7. Excitation winding bracket; 8. Excitation winding bracket; 9. Claw pole; 10.Stator core; 11. Bolts; 12. Pole boots; 13. Permanent magnet steel; 14. Armature winding; 15.Screw; 16. Front end cover; 17. Rotor core; 18. Gasket; 19. Fan; 20. Pulley

A. *Analysis of Leakage Permeance of Brushless Claw Pole Electric Excitation Rotor*

The magnetic flux path diagram of the brushless claw pole electrically excited rotor is shown in Fig. 2, and the equivalent magnetic circuit diagram is shown in Fig. 3 [3, 4].

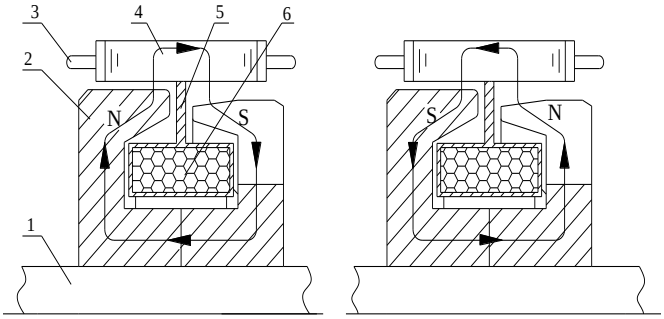

(a) Forward current of excitation winding I_a>0 (b) Reverse current of excitation winding I_a<0

Fig. 2. Flux path diagram of brushless pawless electrically excited rotor.

1. Shaft; 2. N pole claw pole; 3. Armature winding; 4. Stator core; 5. Excitation winding bracket; 6. Excitation winding

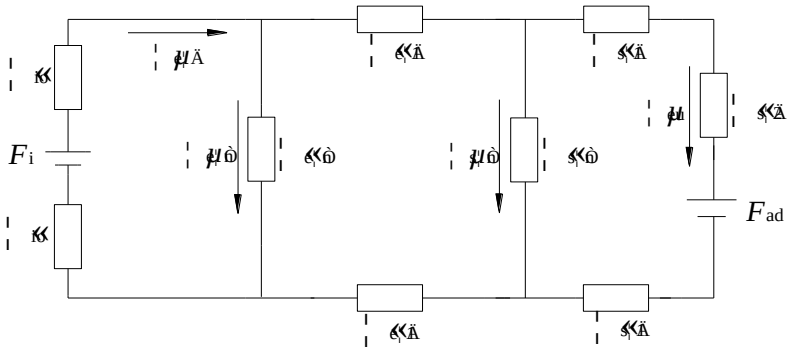

Fig. 3. Equivalent magnetic circuit diagram of claw pole rotor of brushless electric excitation.

In the figure: F_i is the equivalent magnetic potential of the electric excitation winding; Λ_{io} is the equivalent internal permeance of the claw pole of the electric excitation; $\Phi_{e\delta}$ is the total magnetic flux provided for the electric excitation winding; $\Phi_{e\sigma n}$ is the combined leakage magnetic flux between the claw poles of the electric excitation; $\Lambda_{e\sigma n}$ is the synthesis of magnetic leakage permeance between electrically excited pawl poles; $\Lambda_{e\delta 1}$ is the main air gap permeance of the claw pole; $\Phi_{s\sigma n}$ is the magnetic flux leakage between the stator teeth; $\Lambda_{s\sigma n}$ is the leakage permeance between the stator teeth; $\Lambda_{s\delta 1}$ is the stator tooth permeance; Φ_{eu} is the effective magnetic flux through the air gap; $\Lambda_{s\delta 2}$ is the stator yoke permeance ; F_{ad} is the longitudinal component of armature reaction magnetic potential.

The magnetic flux equations are listed according to Kirchhoff's law and Ohm's law of the magnetic circuit:

$$\begin{cases} \Phi_{e\delta} = \Phi_{e\sigma n} + \Phi_{s\sigma n} + \Phi_{eu} \\ F_i = \Phi_{e\delta}\dfrac{2}{\Lambda_{io}} + \Phi_{e\sigma n}\dfrac{1}{\Lambda_{e\sigma n}} \\ \Phi_{e\sigma n}\dfrac{1}{\Lambda_{e\sigma n}} = \left(\Phi_{e\delta} - \Phi_{e\sigma n}\right)\dfrac{2}{\Lambda_{e\delta 1}} + \Phi_{s\sigma n}\dfrac{1}{\Lambda_{s\sigma n}} \\ \Phi_{s\sigma n}\dfrac{1}{\Lambda_{s\sigma n}} = \Phi_{eu}\left(\dfrac{2}{\Lambda_{s\delta 1}} + \dfrac{1}{\Lambda_{s\delta 2}}\right) + F_{ad} \end{cases} \quad (1)$$

(1) Synthetic leakage permeance between claw poles of brushless claw pole electro excitation rotor $\Lambda_{e\sigma n}$

The dimension constraint diagram of brushless claw pole electro excitation rotor is shown in Fig. 4, and the leakage flux distribution diagram is shown in Fig. 5.

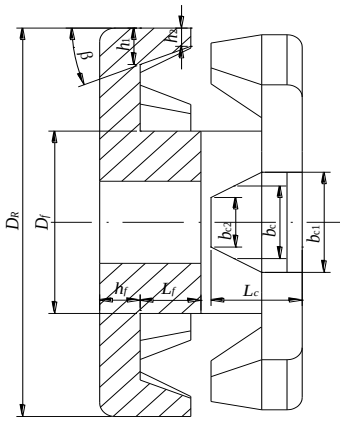

Fig. 4. Dimension constraint diagram of brushless claw pole electro excitation rotor.

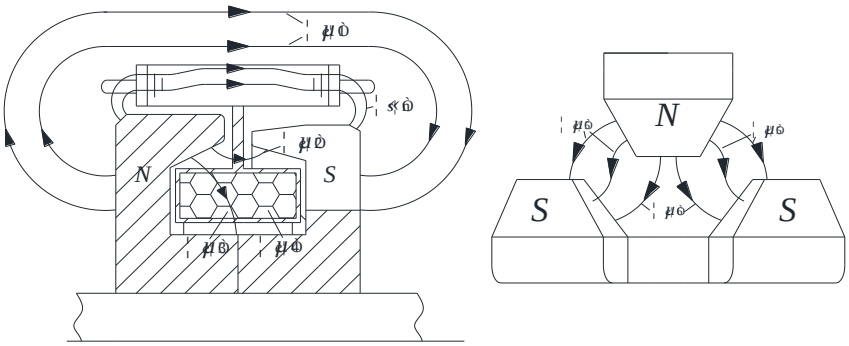

Fig. 5. Distribution of leakage magnetic flux of brushless claw pole electro excitation rotor.

In the picture, $\Phi_{e\sigma 1}$ ——The leakage magnetic flux between the outer end faces of the two claw pole conducting permeance disks; $\Phi_{e\sigma 2}$ ——Magnetic flux leakage between the two claw pole cant; $\Phi_{e\sigma 3}$ ——Leakage magnetic flux between claw pole and cylindrical yoke; $\Phi_{e\sigma 4}$ ——The leakage magnetic flux between the two claw pole yokes passing through the excitation winding space; $\Phi_{e\sigma 5}$ ——The leakage magnetic flux between the two sides of claw pole; $\Phi_{e\sigma 6}$ ——The leakage magnetic flux between the top end face of claw pole and the side of adjacent claw pole.

$$\Lambda_{e\sigma n} = \Lambda_{e\sigma 1} + \Lambda_{e\sigma 2} + \Lambda_{e\sigma 3} + \Lambda_{e\sigma 4} + \Lambda_{e\sigma 5} + \Lambda_{e\sigma 6} \tag{2}$$

- The leakage permeance between the outer end faces of the two claw pole conducting permeance disks $\Lambda_{e\sigma 1}$

$$\Lambda_{e\sigma 1} = \mu_0 \frac{\pi (D_R - 2r)^3}{96 \int_0^{\frac{D_R - 2r}{2}} (\pi h + h_f + L_f)\, dh} \tag{3}$$

In the formula, μ_0 ——permeability of vacuum, $\mu_0 = 4\pi \times 10^{-7} H/m$; D_R ——Outer diameter of claw pole rotor; r ——Shaft radius; h_f ——Flange side thickness; L_f ——Length of claw pole yoke.

- Leakage permeance between the inclined planes of two claw pole $\Lambda_{e\sigma 2}$

Due to the spatial complexity of the leakage permeance between the two claw pole inclined planes, the vertical plane of the claw pole inclined plane was taken as XOY plane and the point with the same distance from the top of the two teeth was taken as the origin. In the absence of the parametric equation of magnetic force lines, the general method for calculating the arc length of the space curve [5] could be used to obtain:

$$\begin{cases} y = 2h\cos\theta \ \left(\theta \in \left[\beta - 90^{O}, 90^{O} - \beta\right]\right) \\ L = \int_{\beta-90^{0}}^{90^{0}-\beta} \dfrac{1}{\cos\varphi}\sqrt{1+\left[y'(\theta)\right]^{2}}\,d\theta \\ \Lambda_{e\sigma 2} = \mu_0 \dfrac{(b_{c1}+b_{c2})(L_c - h_f)}{2\int_{h2}^{(L_c-h_f)/\cos\beta} Ldh}\left(\dfrac{L_c - h_f}{\cos\beta} - h_2\right) \end{cases} \tag{4}$$

In the formula, φ ——the included angle between the space curve and xoy plane; b_{c1} ——width of tooth root of claw pole; b_{c2} ——width of tip tooth of claw pole; L_c ——Axial length of claw pole teeth; h_2 ——thickness of tip tooth of claw pole; β ——angle between claw tip of claw pole.

- Leakage permeance between claw pole and cylindrical yoke $\Lambda_{e\sigma 3}$

$$\begin{cases} r_1 = \left(\dfrac{D_R - D_f}{2} - h_1\right) \Big/ \sin\beta \\ r_2 = r_1 + \left(L_c - h_f\right) \Big/ \cos\beta \\ \Lambda_{e\sigma 3} = \mu_0 \dfrac{(b_{c1}+b_{c2})(L_c - h_f)}{2\int_{r_1}^{r_2} \beta r dr}\left(r_2 - r_1\right) \end{cases} \tag{5}$$

In the formula, D_f ——outer diameter of yoke; h_1 ——Tooth root thickness of claw pole;

- The leakage Magnetic flux between the two claw pole yokes passing through the excitation winding space $\Lambda_{e\sigma 4}$

$$\Lambda_{e\sigma 4} = \mu_0 \frac{\left(D_R - D_f - 2h_1\right) b_{c1}}{4L_f} \tag{6}$$

- The leakage permeance between the two sides of claw pole $\Lambda_{e\sigma 5}$

$$\Lambda_{e\sigma 5} = \mu_0 \frac{\left(h_1 + h_2\right) L_f}{2\sqrt{\left(b_{c3}\right)^2 + \left(L_i\right)^2}\sin\gamma} \tag{7}$$

In the formula, b_{c3} ——Circumferential distance between the top point and the bottom end point of claw pole rotor, $b_{c3} = \frac{b_{c1} - b_{c2}}{2}$; L_i ——The axial distance from the root of claw pole rotor to the top of relative claw pole, $L_i = 2L_f + h_f - L_c$; γ ——Side inclination angle of claw pole rotor, $\gamma = \arctan\frac{L_c - h_f}{b_{c3}}$.

- The leakage permeance between the top end face of claw pole and the side of adjacent claw pole $\Lambda_{e\sigma 6}$

$$\begin{cases} r_1 = L_i \tan\gamma + b_{c3} \\ r_2 = r_1 + b_{c2} \\ \Lambda_{e\sigma 6} = \mu_0 \dfrac{h_2 \cdot b_{c2}}{\int_{r_1}^{r_2} \left(\dfrac{\pi}{2} - \alpha\right) r dr} (r_2 - r_1) \end{cases} \tag{8}$$

(2) Leakage permeance between stator teeth $\Lambda_{s\sigma n}$

The schematic diagram of stator slot type and stator teeth of power generation device is shown in Fig. 6.

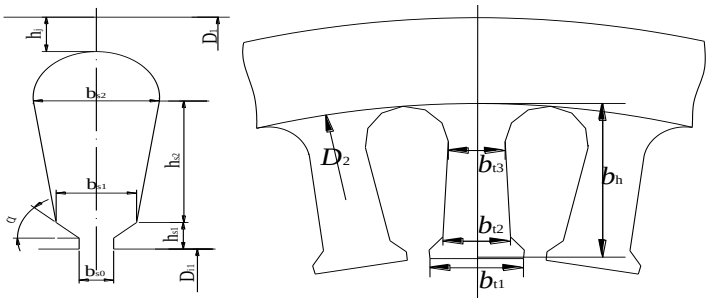

Fig. 6. The schematic diagram of stator slot type and stator teeth of power generation device.

$$\Lambda_{s\sigma n} = \frac{\mu_{r2} \cdot \mu_0}{2(h_f + L_f)} \left\{ \frac{\pi}{12} \left(\frac{D_1^2}{4} + \frac{D_{i1}^2}{4} \right) - \frac{3}{2} \left[\frac{\pi b_{s2}^2}{4} + (b_{s2} + b_{s1}) h_{s2} + (b_{s1} + b_{s0}) h_{s1} + 2h_{s0} \cdot b_{s0} \right] \right\} \tag{9}$$

In the formula, μ_{r2} ——relative permeability of silicon steel sheet, $\mu_{r2} = 8000$; D_1 ——stator outer diameter; D_{i1} ——stator inner diameter; b_{s2} ——width of trapezoidal large end of stator slot; b_{s1} ——width of trapezoidal small end of stator slot; b_{s0} ——stator slot width; h_{s2} ——trapezoidal height of stator slot; h_{s1} ——height of stator slot shoulder; h_{s0} ——stator slot height.

B. *Leakage Permeance Analysis of Radial Permanent Magnet Rotor*

The flux path diagram of the radial permanent magnet rotor is shown in Fig. 7, and the equivalent flux path diagram is shown in Fig. 8.

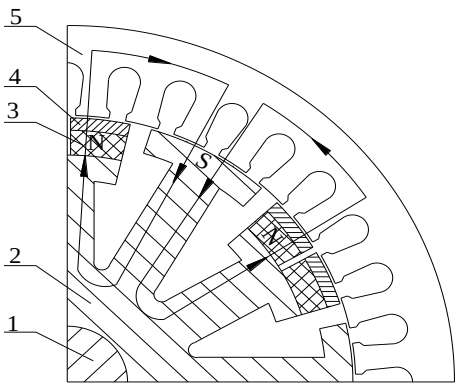

Fig. 7. The flux path diagram of the radial permanent magnet rotor.

1. Shaft; 2. Salient pole rotor core; 3. Permanent magnet steel N-pole; 4. Pole boots; 5. Stator core

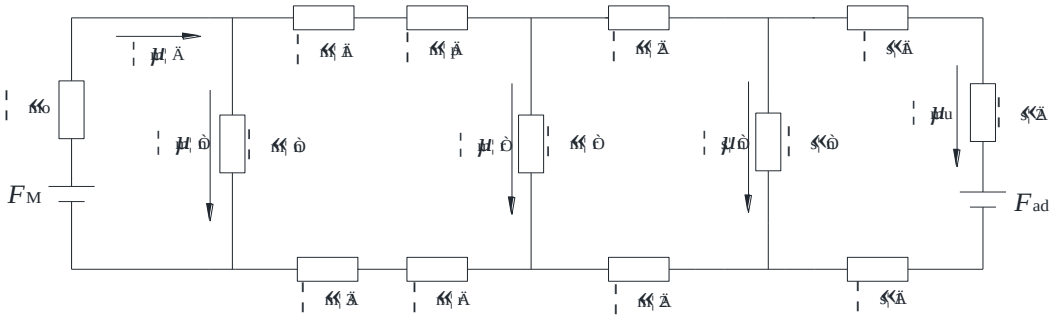

Fig. 8. Equivalent magnetic circuit diagram of radial permanent magnet rotor.

In the figure, F_M is the Equivalent magnetic potential of tile-shaped permanent magnetic steel; Λ_{mo} is equivalent internal permeance of tile-shaped permanent magnetic steel; $\Phi_{m\delta}$ is the total magnetic flux of tile - shaped permanent magnetic steel; $\Phi_{m\sigma n}$ is the composite flux leakage between two end faces of tile-shaped permanent magnetic steel; $\Lambda_{m\sigma n}$ is the composite leakage permeance between two end faces of tile-shaped permanent magnetic steel; $\Lambda_{m\delta 1}$ is additional air gap permeability between tile shaped permanent magnetic steel and pole shoe; $\Lambda_{m\delta p}$ is the pole shoe permeance; $\Phi_{m\sigma r}$ is the leakage magnetic flux between the pole shoe and the adjacent invisible magnetic pole; $\Lambda_{m\sigma r}$ is the leakage permeance between the pole shoe and the adjacent invisible poles; $\Lambda_{m\delta 2}$ is the main air gap permeance between permanent magnet rotor and stator; Φ_{mu} is the effective magnetic flux through the air gap; $\Lambda_{m\delta r}$ is the permeance of the rotor core; $\Lambda_{m\delta 3}$ is the additional air gap permeance between the rotor core and the tile-shaped permanent magnetic steel.

The magnetic flux equations are listed according to Kirchhoff's law and Ohm's law of the magnetic circuit:

$$\begin{cases} \Phi_{m\delta} = \Phi_{m\sigma n} + \Phi_{m\sigma r} + \Phi_{s\sigma n} + \Phi_{mu} \\ F_M = \Phi_{m\delta} \cdot \dfrac{1}{\Lambda_{mo}} + \Phi_{m\sigma n} \cdot \dfrac{1}{\Lambda_{m\sigma n}} \\ \Phi_{m\sigma n} \cdot \dfrac{1}{\Lambda_{m\sigma n}} = \left(\Phi_{m\delta} - \Phi_{m\sigma n}\right)\left(\dfrac{1}{\Lambda_{m\delta 1}} + \dfrac{1}{\Lambda_{m\delta p}} + \dfrac{1}{\Lambda_{m\sigma r}} + \dfrac{1}{\Lambda_{m\delta 3}}\right) + \Phi_{m\sigma r}\dfrac{1}{\Lambda_{m\sigma r}} \\ \Phi_{m\sigma r}\dfrac{1}{\Lambda_{m\sigma r}} = \left(\Phi_{m\delta} - \Phi_{m\sigma n}\right)\dfrac{2}{\Lambda_{m\delta 2}} + \Phi_{s\sigma n}\dfrac{1}{\Lambda_{s\sigma n}} \\ \Phi_{s\sigma n}\dfrac{1}{\Lambda_{s\sigma n}} = \Phi_{mu}\left(\dfrac{2}{\Lambda_{s\delta 1}} + \dfrac{1}{\Lambda_{s\delta 2}}\right) + F_{ad} \end{cases} \tag{10}$$

The size constraint diagram of radial permanent magnet rotor is shown in Fig. 9.

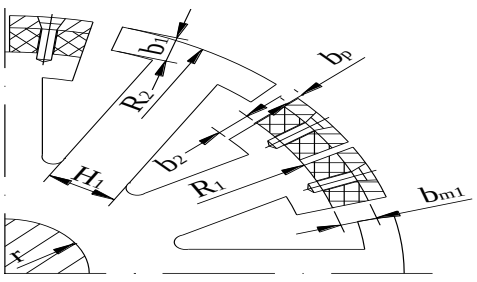

Fig. 9. The size constraint diagram of radial permanent magnet rotor.

(1) Converted to the composite leakage permeance between the two end faces of tile permanent magnet steel $\Lambda_{m\sigma n}$

$$\Lambda_{m\sigma n} = \Lambda_{m\sigma 1} + \Lambda_{m\sigma 2} + \Lambda_{m\sigma 3} \tag{11}$$

① The leakage magnetic flux between the two ends of the tile-shaped permanent magnet steel in the axial direction $\Lambda_{m\sigma 1}$

$$\Lambda_{m\sigma 1} = 0.125\mu_0 h_{\mathrm{ml}} \tag{12}$$

In the formula, h_{m1}——the width of tile-shaped permanent magnet steel.

② The leakage permeance between the sides of the tile-shaped permanent magnet steel $\Lambda_{m\sigma 2}$

$$\Lambda_{m\sigma 2} = \mu_0 \frac{l_{m1}}{\pi}\left[\left(\frac{a_2}{a_2 - a_1}\ln\frac{a_2}{a_1}\right) - 1\right] \tag{13}$$

In the formula, l_{m1}——the axial length of tile-shaped permanent magnetic steel; a_1——the inner diameter pole arc length of tile shaped permanent magnetic steel, $a_1 = \frac{\theta_1 \pi}{180} R_1$; θ_1——the included Angle of tile shaped permanent magnetic steel arc length, R_1——the short salient pole radius of the rotor core; a_2——length of outer diameter pole arc of tile-shaped permanent magnetic steel, $a_2 = \frac{\theta_1 \pi}{180}(R_1 + R_{m1})$, b_{m1}——thickness of the magnetizing direction of tile-shaped permanent magnetic steel.

③ Leakage permeance of non magnetic screw $\Lambda_{m\sigma 3}$

$$\Lambda_{m\sigma 3} = \mu_{r4}\mu_0 \frac{\pi d_{ld}^2}{4 l_{ld}} \tag{14}$$

In the formula, μ_{r4}——relative permeability of stainless steel, $\mu_{r4} = 1.3$; d_{ld}——diameter of non magnetic screw; l_{ld}——effective length of screw.

(2) Leakage permeance between the pole boot and the adjacent invisible pole S pole $\Lambda_{m\sigma r}$

$$\Lambda_{\mathrm{m}\delta p} = \mu_0 \frac{l_{ml}}{\theta_2} \ln \frac{R_2}{R_1 + b_{ml}} \tag{15}$$

In the formula, θ_2—— the included Angle between the pole shoe and the adjacent invisible magnetic pole S pole, $\theta_2 = \frac{1}{6}(1 - \alpha_p)\pi$, in the formula, α_p is the polar arc coefficient; R_2——radius of long salient pole of rotor core.

The magnetic field of the compound excitation power generation device is established by the electric excitation winding and permanent magnet steel, and their magnetic circuits are basically independent of each other. The radial permanent magnetic field provides the main magnetic field of the compound excitation power generation device. As the regulating magnetic field of the compound excitation power generation device, the electric excitation magnetic field can adjust the size of the synthetic magnetic field in the generator by adjusting the current size and direction in the excitation winding, Thus, the output voltage of the power generation device

can be kept stable [6,7].

No load flux leakage coefficient of the compound excitation power generation device σ

$$\sigma = \frac{\Phi_{e\delta} + \Phi_{m\delta}}{\Phi_{eu} + \Phi_{mu}} = 1 + \frac{\Phi_{e\sigma n} + \Phi_{m\sigma n} + \Phi_{m\sigma r} + 2\Phi_{s\sigma n}}{\Phi_{eu} + \Phi_{mu}} \tag{16}$$

It can be obtained from formula (1), (10) and (16):

$$\sigma = 1 + \frac{\left(F_i - \Phi_{e\delta}\frac{2}{\Lambda_{i0}}\right)\Lambda_{e\sigma n} + \left(\Phi_{m\delta}\frac{2}{\Lambda_{m\delta 2}} + \Phi_{s\sigma n}\frac{1}{\Lambda_{s\sigma n}}\right)\Lambda_{m\sigma r} + \left(F_M - \Phi_{m\delta}\cdot\frac{1}{\Lambda_{m0}}\right)\left(\Lambda_{m\sigma r} - \frac{2}{\Lambda_{m\sigma r}\Lambda_{m\delta 2}}\right)\Lambda_{m\sigma n} + 2\Phi_{s\sigma n}}{\Phi_{eu} + \Phi_{mu}} \tag{17}$$

Through the electromagnetic analysis of the composite excitation power generation device, the main parameters affecting the magnetic leakage coefficient are: the width of claw pole tooth root b_{c1} width of claw pole tooth top b_{c2} thickness of claw pole tooth top h_2 and thickness of flange side h_f of the electro excitation rotor, the thickness of the tile-shaped permanent magnetic steel of the permanent magnet rotor in the magnetizing direction b_{m1}, the polar arc coefficient α_p, etc. In this paper, the electric excitation rotor adopts a variable section, isosceles trapezoidal clawed pole structure to reduce magnetic leakage, and the permanent magnet rotor adopts a segmented invisible pole structure to improve the material utilization rate.

III. Parameter Optimization and Simulation Analysis of the Compound Excitation Power Generation Device

A. *Parameter Optimization*

Particle swarm optimization (PSO) [8] is an efficient optimization technology that simulates animal foraging behavior and seeks the optimal solution through individual cooperation, and has the characteristics of few parameters, simple concept and easy implementation [9, 10].

Based on the characteristics of the main structural parameters of the composite excitation power generation device, taking the mathematical model established by the permeance analysis of the composite excitation power generation device as the objective function, the particle swarm optimization algorithm is used to optimize the main structural parameters of the rotor of the composite excitation power generation device.

(1) According to the analysis of leakage permeance, a mathematical model is established, which takes the main parameters ($b_{c1}, b_{c2}, h_2, h_f, b_{m1}, \alpha_p$) which affect the magnetic leakage coefficient as the optimization design variable. The relationship between the structure parameters and the optimization objectives of the composite excitation power generation device which needs to be optimized can be expressed as follows:

$$\begin{cases} \min & \sigma = f(b_{c1}, b_{c2}, h_2, h_f, b_{m1}, \alpha_p) \\ & 21.0 \le b_{c1} \le 23.0 \\ & 10.0 \le b_{c2} \le 14.0 \\ & 4.0 \le h_2 \le 8.0 \\ s.t. & 12.0 \le h_f \le 16.0 \\ & 2.0 \le b_{m1} \le 4.0 \\ & 0.65 \le \alpha_p \le 0.80 \end{cases} \tag{18}$$

(2) Selection of constraints. The range of design variables is determined according to the variation interval between the maximum and minimum values of the empirical value of the variable in engineering design.

(3) Abnormal data processing is not feasible. In the process of optimization, there may be unreasonable data combination or iterative non-convergence in the optimization process. Therefore, the paper should take into account the influence of generator materials and manufacturing factors, and make appropriate adjustments in the optimization of the generator. The optimization results of PSO and the independent design results of permanent magnet and electric excitation by using the generator design expert system are shown in Table 3.

Table 1. Comparison of optimization results.

	b_{c1}	b_{c2}	h_2	h_f	b_{m1}	α_p	σ
PSO algorithm	21.837	10.035	3.263	12.884	3.523	0.675	1.3384
expert system	22.0	10.0	3.5	12.0	3.0	0.70	1.3445
Rounding result	22.0	10.0	3.0	13.0	3.5	0.68	1.3402

By analyzing the data in Table 1, it can be seen that the optimization result is macroscopic consistent with the generator expert system design result, and the magnetic flux leakage coefficient has been improved to some extent after optimization. The structural parameters of the final composite excitation power generation device are obtained according to the actual size and rounded optimization results that the generator can satisfy.

B. *Simulation Analysis*

The mathematical model of magnetic field analysis is established according to Maxwell equations [11]:

$$\begin{cases} \oint_l H \cdot dl = \int_S (J + \dfrac{\partial D}{\partial t}) \cdot dS \\ \oint_l E \cdot dl = -\int_S \dfrac{\partial B}{\partial t} \cdot dS \\ \oint_S B \cdot dS = 0 \\ \oint_S D \cdot dS = \int_V \rho \cdot dV \end{cases} \tag{19}$$

In the above equations, the relationship between field quantities is: $D = \varepsilon E$, $B = \mu H$, $J = \sigma E$, D is the electric displacement vector, E is the electric field intensity, B is the magnetic induction intensity, H is the magnetic field intensity, J is the current density, ρ is the charge density.

By establishing three-dimensional geometric model, defining material properties, boundary conditions, and then loading the excitation source and solving and post-processing. Because of the circumferential symmetry of the generator rotor structure, each pair of magnetic poles is a circulating unit, so the 1/6 model of the rotor is established. 3D co-simulation was conducted for the composite excitation power generation device. When positive excitation source was loaded, the stator internal flux density vector diagram and flux density cloud diagram were shown in Fig. 10; when reverse excitation source was loaded, the stator internal flux density vector diagram and flux density cloud diagram were shown in Fig. 11.

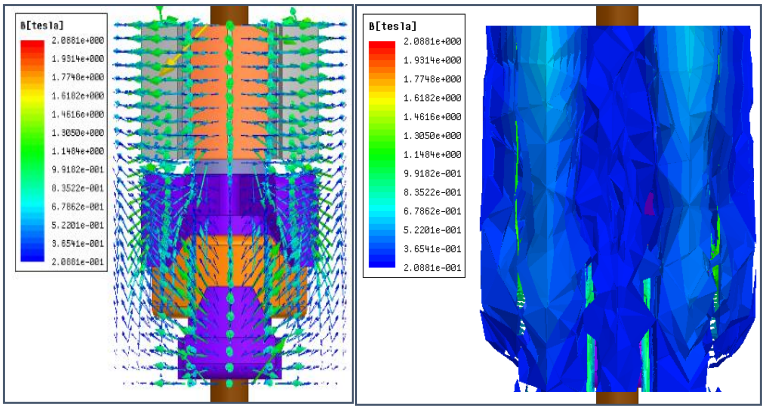

Fig. 10. Vector diagram and cloud diagram of flux density in stator when forward excitation source is loaded.

It can be seen from Fig. 10 that when the positive excitation current is applied to the electric excitation winding, the direction of the magnetic line of force generated is the same as that generated by the permanent magnet steel. When the electric excitation magnetic field and the permanent magnetic field are superimposed, the magnetic flux density in the generator stator winding increases and the output voltage increases.

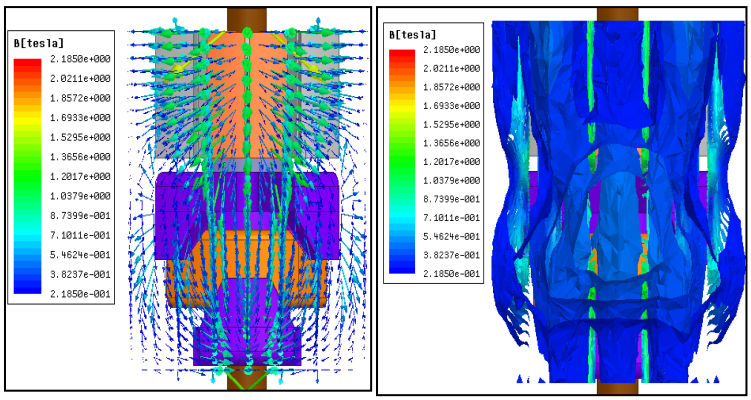

Fig. 11. Vector diagram and cloud diagram of flux density in stator when reverse excitation source is loaded.

As can be seen from Fig. 11, when the electric excitation winding provides reverse excitation current, the direction of the magnetic force line generated is opposite to that generated by the permanent magnetic steel. The electric excitation magnetic field weakens the permanent magnetic field, the flux density in the generator stator winding decreases, and the output voltage decreases.

Through the analysis of the flux density vector in the air gap, it can be seen that the flux density in the stator winding of the composite excitation power generation device, can be adjusted by adjusting the magnitude and direction of the current in the electric excitation winding, so as to achieve the purpose of output stable voltage of the composite excitation power generation device.

IV. PERFORMANCE TEST

The brushless electromagnetic and radial permanent magnet composite excitation stabilized voltage generation device used for automobile is the 12-pole three-phase synchronous generator. The permanent magnetic steel is NdFeB NTP30H [12]. Its remanent magnetic induction strength Br = 1.2T, magnetic field strength Hc = 790kA/m, and the maximum magnetic energy product (BH) Max = 224-256kJ /m3. The width of the claw pole tooth root of the electric excitation rotor is 22mm, the width of the claw pole tooth top is 10mm,

the thickness of the claw pole tooth top is 3mm, and the thickness of the flange side is 13mm. The thickness of the magnetizing direction of the tile permanent magnetic steel of the permanent magnet rotor is 3.5mm, and the pole arc coefficient is 0.68. The rated voltage and power of the composite excitation generator are 28V and 1000W, rated speed 4000r/min. Under the condition of load power of 900W, 1000W and 1100W respectively, the performance test of the newly developed compound excitation stabilized voltage generation device was carried out from low speed to high speed. The test results are shown in Table 2.

Table 2. Test results of output voltage of the power generation device /V.

Power/W / Speed/r/min	900	1000	1100
2000	27.1	26.6	25.8
4000	28.3	28.4	28.3
6000	28.6	28.6	28.5

V. CONCLUSION

(1) The equivalent magnetic circuit method is used to draw the equivalent magnetic circuit diagram of the composite excitation power generation device, the derivative model of the rotor leakage permeance of the power generation device is established, the influencing factors of leakage permeance are analyzed, measures are taken to suppress magnetic flux leakage, reduce magnetic flux leakage and improve the power generation efficiency.

(2) Taking the rotor flux leakage coefficient of the composite excitation power generation device as the objective function, the particle swarm optimization algorithm was adopted to optimize the main structural parameters of the generator to obtain the optimal matching parameters.

(3) The composite excitation power generation device with no carbon brush slip ring structure and low failure rate is developed. When the rotating speed changes from 2000r/min to 4800r/min and the load power changes from 900W to 1100W, the output voltage is stable within the range of 25.8V ~ 28.6V, and the voltage stabilization effect is good.

REFERENCES

[1] Shi Liwei, Zhang Shaohong, Zhang Xueyi. Automotive electrical appliances [M]. Beijing: National Defense Industry Press, 2011, 04:254.
[2] MA Youliang. Automotive Electrical and electronic control system [M]. Beijing: China Machine Press, 2020, 01: 505.
[3] Tang Renyuan. Theory and design of modern permanent magnet motor [M]. Beijing: China Machine Press, 2020: 13-35.
[4] Wang Qunjing, NI Youyuan, LI Guoli. Structure, theory and application of claw pole motor[M]. Hefei: China University of science and Technology Press, 2006: 44.
[5] Zhang Ting, Zhang Zhihong, SUN Mingbao. Transplantation of a single variable integral formula to multiple integral and its application [J]. Journal of Hunan Institute of Technology, 2015,28(02):21-26.
[6] Zhang Zhuoran, Wang Dong, Hua Wei. Review and Prospect of structure principle, design and operation control technology of hybrid excitation motor [J]. Chinese Journal of Electrical Engineering.2020, 40(24):7834-7850.
[7] Zhang Xueyi. Research on the technology of using permanent magnet and electromagnetic hybrid excitation power generation system to recover automobile exhaust residual energy [D]. Doctoral Dissertation of Shandong University of science and technology, 2011, 12:74-84.
[8] Kennedy J, Eberhart RC.Particle swarm optimization[C]// Proceeding of IEEE International Conference on Neural Networks. Piscataway: IEEE Press,1995:1492-1498.
[9] LI Li, NIU Ben. Particle swarm optimization algorithm [M]. Beijing: Metallurgical Industry Press, 2009.10:25-31.
[10] YU Ying, LI Yongsheng, YU Xiaochun. Application of particle swarm optimization in engineering optimization design[J]. Journal of Mechanical Engineering, 2008(12):226-231.
[11] Zhang Xueyi, DU Qingjun, MA Shilun. Development of Automobile Hybrid Excitation Generator [J]. Automotive Engineering. 2017, 39(07):822-826.
[12] LI Zhongming. Rare earth permanent magnet motor[M]. Beijing: National Defense Industry Press, 1999, 07:15-22.

AUTHOR'S PROFILE

First Author
Mingjun Xu, Master in reading, Male, School of Transportation and Vehicle Engineering, Shandong University of Technology, Shandong, Zibo, 255000, China.

Second Author
Hongbin Yin, Doctor of Engineering, Male, School of Transportation and Vehicle Engineering, Shandong University of Technology, China, Shandong, Zibo, 255000 (Correspondence author).

Third Author
Shilong Yan, Master in reading, Male, School of Transportation and Vehicle Engineering, Shandong University of Technology, Shandong, Zibo, 255000, China.

Fourth Author
Yanhong Gao, Female, Shandong Tangjun Ouling Automobile Manufacturing Co. Ltd, Zibo City, Shandong Province, 255000, China.

Fifth Author
Zhendong Liu, Master in reading, Male, School of physics and electronic information, Dezhou University, Shandong, Dezhou, 253000, China.

Sixth Author
Wenchao Zhang, Master in reading, Male, School of Transportation and Vehicle Engineering, Shandong University of Technology, Shandong, Zibo, 255000, China.